

Geophysical Research Letters

RESEARCH LETTER

10.1029/2019GL084759

Key Points:

- We report the first identification of Quasi-Biennial Oscillation in Antarctic planetary waves & QBO dipole-cell pattern in polar night jet
- Additional processes to the Holton-Tan effect may play a role in transmitting the equatorial QBO signal into the Antarctic zonal-mean winds
- QBO signal is imposed by enhancing the polar night jet poleward of 55°S and its instability, generating EPWs with larger growth rate in QBOe

Supporting Information:

- Supporting Information S1

Correspondence to:

X. Lu,
xianl@clemson.edu

Citation:

Lu, X., Wu, H., Chu, X., Oberheide, J., Mlynczak, M. G., & Russell, J. M., III (2019). Quasi-biennial oscillation of short-period planetary waves and polar night jet in winter Antarctica observed in SABER and MERRA-2 and mechanism study with a quasi-geostrophic model. *Geophysical Research Letters*, 46, 13,526–13,534. <https://doi.org/10.1029/2019GL084759>

Received 30 JUL 2019

Accepted 8 NOV 2019

Accepted article online 12 NOV 2019

Published online 22 NOV 2019

Quasi-Biennial Oscillation of Short-Period Planetary Waves and Polar Night Jet in Winter Antarctica Observed in SABER and MERRA-2 and Mechanism Study With a Quasi-Geostrophic Model

Xian Lu¹ , Haonan Wu¹ , Xinzhaoh Chu² , Jens Oberheide¹ , Martin G. Mlynczak³ , and James M. Russell III⁴

¹Department of Physics and Astronomy, Clemson University, Clemson, SC, USA, ²Cooperative Institute for Research in Environmental Sciences and Department of Aerospace Engineering Sciences, University of Colorado Boulder, Boulder, CO, USA, ³NASA Langley Research Center, Hampton, VA, USA, ⁴Center of Atmospheric Science, Hampton University, Hampton, VA, USA

Abstract Analyzing Sounding of the Atmosphere using Broadband Emission Radiometry (SABER) observations from 2003 to 2018, the interannual variability of 2–5d eastward propagating planetary waves is found to correlate positively with zonal-mean zonal winds averaged over $67.5^{\circ}\pm10^{\circ}$ S but negatively with the quasi-biennial oscillation (QBO) index in austral winter. The composite-mean wave amplitudes are ~20% larger in QBOe than in QBOw. On statistical average, the poleward flank strengthening and the equatorward flank weakening of polar night jet (PNJ) during QBOe form a dipole-cell pattern. In contrast, only a single negative cell is seen in the Northern Hemisphere zonal-mean zonal winds (January) previously explained by the Holton-Tan theory. Such difference implies an interhemispheric asymmetry and other processes needed to explain the additional positive cell in Antarctica. Mechanistic modeling illustrates that the stronger PNJ generates eastward propagating planetary waves with larger growth rates (stronger waves) in QBOe than QBOw, explaining the QBO-like signal in the Antarctic planetary waves.

1. Introduction

The short-period (2–5 days) planetary Rossby waves propagating eastward relative to the ground (eastward propagating planetary waves, EPWs) cause significant perturbations and day-to-day variability in the dynamics, chemistry, and composition of the stratosphere and mesosphere in winter Antarctica (e.g., Alexander & Shepherd, 2010; Allen et al., 1997; Baumgaertner et al., 2008; Coy et al., 2003; Lawrence et al., 1995; Manney et al., 1998). They also impose significant momentum deposition and eastward acceleration to the mean flow and play a dominant role in driving the general circulation of the polar mesosphere (Becker, 2017; McLandress et al., 2006). The EPWs are generated by barotropic/baroclinic instability of the polar night jet (PNJ) (Manney & Randel, 1993; Watanabe et al., 2009), and a stronger PNJ leads to a larger growth rate of wave amplitudes (Hartmann, 1983). Due to the stronger PNJ in the Southern Hemisphere (SH), the amplitudes of EPWs are also stronger in SH than in the Northern Hemisphere (NH) (Venne & Stanford, 1982). Using the 6-day nearly continuous lidar observations at McMurdo (77.8° S, 166° E), Antarctica, Lu et al. (2017) have found that the EPW vertical coupling extends from the stratosphere to the lower thermosphere, and the amplitude growth of 4-d and 2.5-d waves suggests another wave peak above 110 km. The importance of EPWs in the momentum budget and vertical coupling is indisputable, and their interannual variability, which potentially affects the climate of the polar atmosphere, deserves investigation.

The restoring force of Rossby waves resides in the meridional gradient of planetary vorticity or Coriolis parameter constrained by the conservation of absolute vorticity (Rossby & Collaborators, 1939). Thus, the intrinsic motion of Rossby waves relative to mean flow has to be westward in order to avoid filtering effects (Charney & Drazin, 1961), which explains that the EPWs are confined to high-latitude winter hemisphere where the PNJ sustains strong eastward winds. Satellite observations and meteorological data have shown that the main wave activity occurs poleward of 50°S (Garcia et al., 2005; Lu et al., 2013). In contrast to the phases of stationary planetary waves (SPWs), defined as longitudes with maximum amplitudes, that are constant with time, the EPW phases propagate eastward with time as observed from ground, which gives the definition of eastward propagating waves relative to ground.

The quasi-biennial oscillation (QBO) is the most prominent interannual variability in the equatorial stratosphere resulting from the interactions of the mean flow with equatorial waves including Rossby, Kelvin, and gravity waves (Baldwin et al., 2001). The direct QBO impact on zonal winds centers around the equator and has a Gaussian distribution with a half width of $\sim 12^\circ$ in latitude (Dunkerton & Delisi, 1985). Holton and Tan (1980) first proposed a mechanism to explain the QBO signal in the extratropical wind circulation in the NH winter (November–January): In the westerly phase (QBOw) characterized by eastward equatorial zonal wind, the zero-wind line of SPWs extends to the summer hemisphere, so the wave guide is broader and the SPWs cause less disturbance to the polar vortex, resulting in a stronger PNJ than the easterly phase (QBOe). Numerous observational and modeling studies (e.g., Baldwin & Dunkerton, 1998a; Dunkerton & Baldwin, 1991; Hamilton, 1998; O’Sullivan & Salby, 1990) gave credence to the Holton-Tan mechanism, which was also used to explain a greater number of sudden stratospheric warming events in QBOe when the SPWs are more confined at high latitudes so the polar vortex is weaker and more disturbed (Labitzke, 1982). Unlike the QBO effects on the PNJ well studied in the NH, the SH counterpart was less addressed especially above 50 km; and to the best of our knowledge, the possible QBO effects on the Antarctic EPWs have not been studied before. In this work, we aim to explore these QBO effects in Antarctic winter and their possible mechanisms.

2. Observations and Results

2.1. SABER Observations and MERRA-2 Reanalysis Data

The long-term (2003–2018) Sounding of the Atmosphere using Broadband Emission Radiometry (SABER) observations with their large vertical extent (20–110 km) (Russell et al., 1999) are optimal to study the interannual variability of the EPWs since they fully cover the vertical region where the waves are strong in the middle atmosphere. Due to the yaw cycle of SABER, we choose a 51-day window from day 198 to 248 (late July to early September) during which the waves are strong and measurements are made from 82°S to 52°N for all 16 years. The level-2 data in temperature and geopotential height are first binned and averaged in a grid box of $30^\circ \times 5^\circ \times 2$ km (longitude \times latitude \times altitude) to produce the gridded data for each day, and 51 days of data form a four-dimensional matrix. The two-dimensional fast-Fourier transform in the domain of time and longitude is applied upon the gridded data to derive the amplitudes and phases of different wave components (Lu et al., 2013) at each latitude and altitude grid for each year. The 2–5d EPW1 amplitudes are then computed by averaging the amplitudes of the waves falling into periods of 2–5 days and wave number of -1 (eastward propagating). The periods of 2–5 days represent the most dominant oscillations in the PNJ polar flank (e.g., Hartmann, 1983). Since EPWs are generated as a group with multiple periods such as 2, 4, and 5 days (Allen et al., 1997; Lu et al., 2013, 2017), the amplitude averaging without considering different phases provides an estimation of the overall strength of these waves, or in other words, how efficient the whole group of waves are generated. As the 51-day window length approaches 60 days covering a full diurnal cycle in local time (Zhang et al., 2010), the spectral contamination from atmospheric tides is minimal and the method reasonably captures the wave structure as shown in section 2.3.

The Modern Era-Retrospective Analysis for Research and Applications, version 2 (MERRA-2) reanalysis data (Gelaro et al., 2017) are used to provide zonal-mean zonal winds from surface to the top boundary of 0.01 hPa (~ 80 km) for characterizing the PNJ. MERRA-2 produces a realistic QBO in zonal wind, mean meridional circulation, and ozone over the 1980–2015 time period (Coy et al., 2016). The inclusion of Aura Microwave Limb Sounder temperatures beginning in August 2004 has greatly improved the data quality above 40 km, which overlaps the time window of our interests. The MERRA-2 data are provided on pressure levels (P) that are converted to log-pressure heights (z) by $z = H \log(P_0/P)$, with scale height $H = 7$ km and reference pressure $P_0 = 1,000$ hPa.

2.2. QBO-Like Signals in 2–5d EPW1 Amplitudes and PNJ

Considering that the EPWs are confined to high latitudes that sustain the westward intrinsic wave motion, we average the wave amplitudes in a latitudinal band of 50°–82°S and the results are shown in Figures 1a and 1b for temperature and geopotential height, respectively. Since the SABER observational window is centered around August, we project the results into August of each year. Without any postprocessing, the interannual variability of the 2–5d EPW1 with a cycle of 2–3 years is salient. Stronger waves from 40 to 80 km are seen in

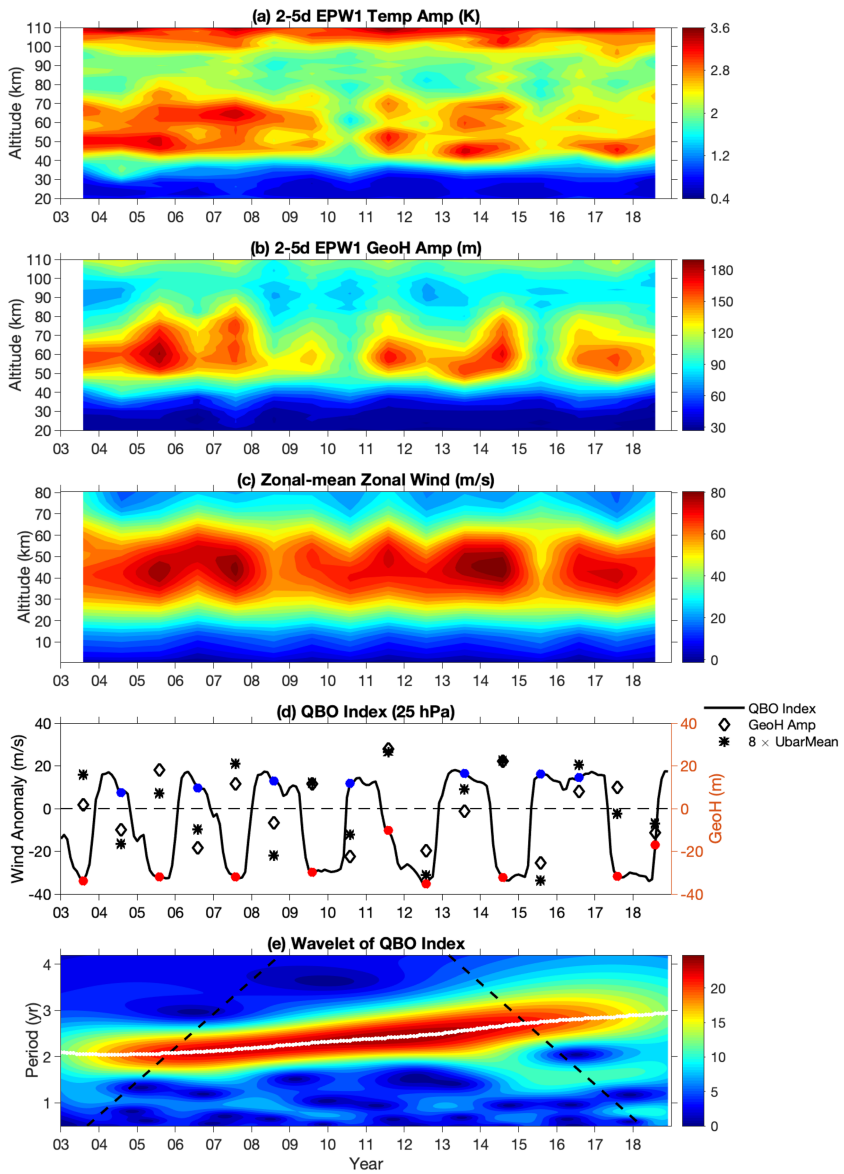


Figure 1. SABER 2–5d EPW1 amplitudes in (a) temperature and (b) geopotential height averaged from 50 to 82°S . (c) MERRA-2 zonal-mean zonal winds averaged between $67.5 \pm 10^\circ\text{S}$ in August. (d) Monthly QBO index (black line), maximum amplitudes in geopotential height (diamonds), and vertically averaged zonal-mean winds multiplied by 8 (stars). Red/blue dots highlight QBOe/QBOW phases. (e) Wavelet spectrum of QBO index. White dots highlight peak periods.

2003, 2005, 2007, 2009, 2011, 2013/2014 for temperature/geopotential height, and 2017, and weaker ones in other years.

To correlate the wave amplitudes with the PNJ, the zonal-mean zonal winds from MERRA-2 are averaged over a month (August) and in a latitudinal band of $67.5^\circ \pm 10^\circ\text{S}$ for each year (Figure 1c). The reason of selecting this band will be given in section 2.3. The interannual variability of the wave amplitude positively follows that of the zonal-mean winds in the range of 25–60 km. Larger wave amplitude unanimously corresponds to stronger zonal-mean winds, and vice versa.

The monthly QBO indices are defined as equatorial zonal-mean zonal winds at 25 hPa and obtained from MERRA-2. The 25-hPa level optimizes the extratropical QBO signal in the SH according to previous studies (Baldwin & Dunkerton, 1998b). In August (Figure 1c), relatively strong 2–5d EPW1 and zonal-mean winds are observed when the QBO indices are negative (easterly phase, red dots in Figure 1d) and the weak ones are found in QBOW (blue dots in Figure 1d) except for 2012, 2013, 2016, and 2018. Despite such

exceptions, the interannual cycles of EPW1 and zonal-mean winds tend to change from 2 to 3 years, following the trend of QBO periods that shifts indeed from 2 to 3 years from 2003 to 2018, according to its wavelet spectrum (Figure 1e).

To further identify the correlation among EPW1 amplitudes, zonal-mean winds, and QBO indices, we take the maximum wave amplitude in geopotential height and vertical mean of zonal-mean zonal winds over 0–80 km altitude as proxies for wave amplitude and background wind, respectively. We apply a high-pass filter with a cutoff frequency of 4 years to remove the long-term interannual variability such as solar cycle. The EPW1 amplitudes are positively correlated with zonal-mean winds with a coefficient of ~ 0.88 and confidence level (CL) of $\sim 100\%$ with all years considered (black diamonds and stars in Figure 1d). The correlation between EPW1 amplitudes and QBO is around -0.49 ($CL = 95\%$), and that between zonal-mean winds and QBO is around -0.35 ($CL = 81\%$) with all years considered. If we consider the first 9 years (2003–2011), these two coefficients become -0.72 ($CL = 97\%$) and -0.82 ($CL = 99\%$), correspondingly. Overall, the 2–5d EPW1 amplitudes closely follow the zonal-mean winds, and both tend to follow the interannual variability corresponding to the QBO with negative correlations, especially before 2012. After 2012, other processes may also play roles in determining the interannual changes of EPW1 and zonal-mean winds.

2.3. Differences between Opposite QBO Phases in Wave Amplitudes and PNJ

To diagnose the QBO-related differences, we separate 16 years into QBOe and QBOw phases. The average of the absolute EPW1 wave amplitudes or zonal-mean zonal winds over the QBOe/QBOw years is referred to as the QBOe/QBOw composite mean, respectively (first and second rows in Figure 2). The high-latitude (poleward of 40° S) waves are EPW1 generated by the PNJ instability, while low-latitude ones ($\pm 30^{\circ}$ S) are ultrafast Kelvin waves excited by tropical convective activity in the lower atmosphere (Chang et al., 2010; Forbes et al., 2009; Gu et al., 2014). The global structure of EPW1 agrees with the previous observations (Allen et al., 1997; Garcia et al., 2005; Lu et al., 2013), meaning that they are robustly extracted. The QBOe corresponds to stronger waves than QBOw (Figures 2a1–2b1, and 2a2–2b2), consistent with the results shown in Figure 1. The maximum amplitudes in temperature reach 3.4 and 3.0 K in QBOe and QBOw around 48 km, while those in geopotential heights are 191.2 and 160.8 m around 56 km, respectively. Similar to the lidar observations (Lu et al., 2017), the EPW1 activity diminishes between 80 and 100 km while resuming above it, implying another peak in the lower thermosphere. The mechanism of the MLT waves is not clear yet. An in situ instability or planetary wave-gravity wave interaction used to explain SPWs in the MLT (Lu et al., 2018; Smith, 2003) are both likely.

Taking the amplitude differences between QBOe and QBOw, the maxima reach ~ 0.4 K in temperature at ~ 48 km and ~ 34.6 m in geopotential height at ~ 56 km (Figures 2a3–2b3), which account for $\sim 20\%$ change of the absolute amplitude in composite mean. To test the statistical significance of amplitude differences, we randomly choose 8 out of 16 years, thereby dividing them into two groups. We take the average amplitudes of each group and calculate their differences. Such a process is repeated for 500 times, and the difference fields are recorded. The means of the difference fields from these 500 samples are close to zero. The QBO-related amplitude differences outside of (or larger than) one standard deviation of these 500 samples are regarded as statistically significant. If only the years of 2003–2011 are considered, the QBOe–QBOw differences are larger reaching 0.6 K and 36.8 m in temperature and geopotential height, respectively, and significant regions are also bigger (Figures 2a4–2b4) than the case with all years considered. The enhancement of the EPW1 activity in QBOe is found from 40–80 km and 50 – 80° S (dashed-line red box). The year-to-year variation in the different QBO phases can be even larger. For instance, the wave amplitude in 2014 (QBOe) is about twice as much as that in 2015 (QBOw) (Figure 1b). The QBO effects in the lower thermosphere are weak for the 2–5d EPW1 in Antarctica but noticeable for the ultrafast Kelvin waves around equator (Figures 2a3–2b3, and 2a4–2b4), which also appear to be stronger in QBOe than QBOw.

In August, the polar flank (southward of 55° S) and core of the PNJ are stronger in QBOe than QBOw (Figures 2c1–2c2), and the differences between them (Figure 2c3) show a dipole-cell structure characterized by a positive cell at high latitude (poleward of 55° S) and a negative cell at midlatitude to low latitude (20 – 55° S). The same significance test as for wave amplitude differences is conducted for the PNJ differences, which shows that the positive cell and part of the negative cell are statistically significant. The positive cell (dashed-line red box in Figure 2c3) causes stronger zonal-mean zonal winds in

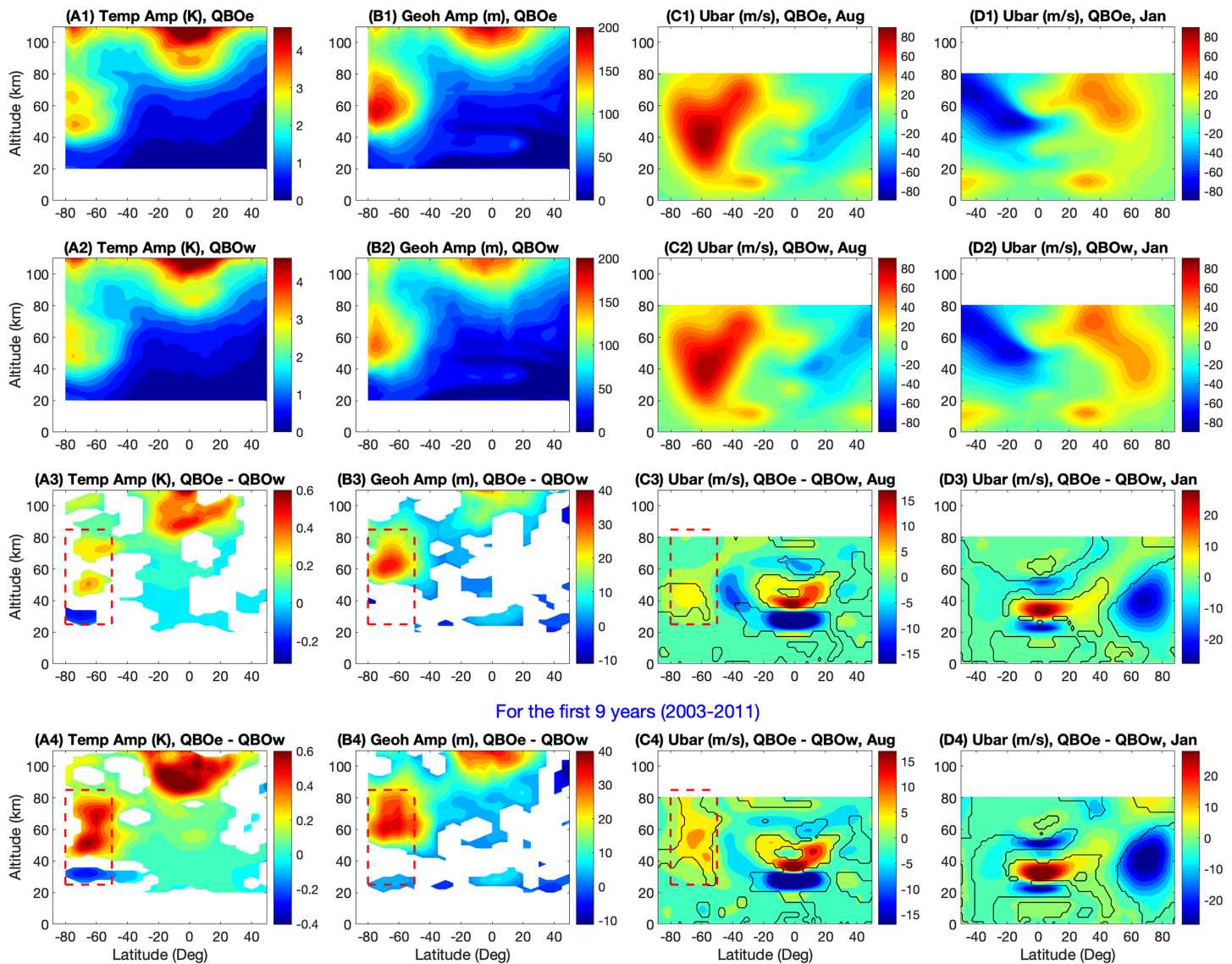


Figure 2. (2a1–2a3) The 2–5d EPW1 amplitudes in temperature in QBOe and QBOw, and differences of QBOe–QBOw. (b–d) The same except for wave amplitudes in geopotential height and \bar{U} in August and January, respectively. (2a4–2d4) The same as 2a3–2d3 except that only the first 9 years are considered. In Figures 2a3–2b3 and 2a4–2b4, only statistically significant results are shown. In Figures 2c3–2d3 and 2c4–2d4, significant regions are enclosed by thin black contours. Dashed-line red boxes in Figures 2a3–2c3 and 2a4–2c4 highlight the regions where enhancements of wave activity and PNJ are both observed.

QBOe than in QBOw at $67.5^\circ \pm 10^\circ\text{S}$. This is why this latitudinal band is selected to produce Figure 1c. Meanwhile, this positive cell corresponds to the wave amplitude enhancement region (also highlighted with red boxes), which explains the positive correlation between EPW1 activity and polar flank PNJ strength in Figure 1. If the first 9 years are considered, the positive cell becomes stronger, the significant region becomes bigger, while the negative cell becomes weaker, than the case with all years considered (Figure 2c4).

The Holton-Tan theory argues that the PNJ in January in the NH should be stronger in QBOw as the wave guide of SPWs is broader; thus, the deceleration effect from the SPW wave drag on the PNJ is smaller than that in QBOe. Considering the *discrepancy* of the NH and the SH winters, we now examine the QBO impact on the PNJ in January. The transition of the QBO phases has a strong preference to occur during April-June (Baldwin et al., 2001); thus, the equatorial zonal-mean zonal winds often show an opposite sign in January compared to August of the same year (Figure 1d). The QBO phase in NH is therefore defined as the zonal-mean wind at 50 hPa (Baldwin et al., 2001) in January. In the NH, the PNJ is indeed statistically stronger in

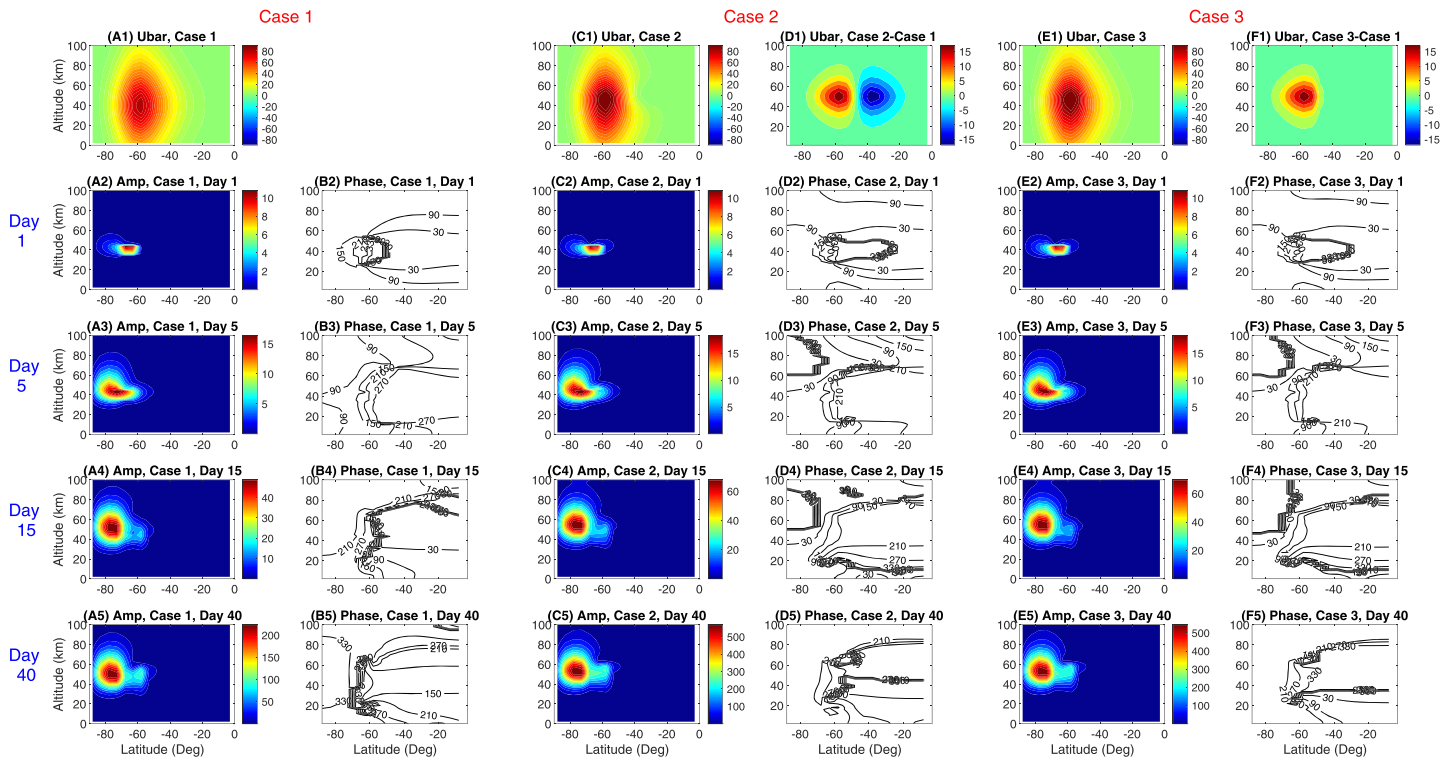


Figure 3. (3a1, 3c1, 3e1) Zonal-mean zonal winds for Cases 1–3, respectively. (3d1 and 3f1) Differences of zonal-mean winds. (3a2, 3c2, 3e2) EPW1 amplitudes for Cases 1–3, respectively. (3b2, 3d2, 3f2) Same as Figures 3a2, 3c2, and 3e2 except for EPW1 phases. Rows 2–5 are for days 1, 5, 15, and 40. The units for zonal-mean wind, wave amplitude, and phase are m/s, m, and degree, respectively.

QBOw as shown by a single negative cell poleward of 40°N and from 20 to 60 km (Figure 2d3), which has been reported by previous observations (Baldwin & Dunkerton, 1998a). This NH January pattern is in strong contrast to the dipole-cell pattern in SH August, which implies that the Holton-Tan mechanism may be applicable to the equatorward flank of the SH PNJ where the negative cell is found but not to Antarctica with the positive cell. Extra dynamical processes may play a role in the southern polar region, which deserves future investigation.

3. A Mechanism Study Using a Linear Quasi-Geostrophic Model

Following the studies by Hartmann (1979, 1983) that simulated the EPW generation by barotropic and baroclinic instability of the PNJ, we use the same linear, spherical, and baroclinic quasi-geostrophic model based on potential vorticity equation to investigate the sensitivity of the unstable planetary-scale normal modes to the background winds in different QBO phases. As described in the supporting information (SI), this mechanistic model assumes a wave form longitudinally therefore reduces to two dimensions (latitude–log-pressure height). The model has grids of $2^{\circ} \times 5\text{ km}$ and proceeds with a time step of 1.5 h. It is adopted to the SH and extends from the surface to 100 km. A radiation condition is applied at the top boundary and zero vertical wind condition at the bottom. The lateral boundary conditions are vanishing wave perturbations. For simplicity, the Newtonian cooling coefficient is taken to be $1/20\text{ day}^{-1}$ and buoyancy frequency squared $N^2 = 4 \times 10^{-4}\text{ s}^{-2}$.

The zonal-mean zonal winds (\bar{u}) required in the potential vorticity equation (A1) of SI is given by an analytical form used in Hartmann (1983) to represent the first-order structure and maintain the required instability for Case 1. The \bar{u} parameters are optimized to largely mimic the strength and position of the PNJ in QBOw (Figure 3a1). Then a dipole-cell pattern (Figure 3d1), also formulated analytically, is added to \bar{u} of Case 1 to produce \bar{u} for Case 2 (Figure 3c1). The differences of model results between Cases 1 and 2 therefore stem from the dipole pattern related to the QBO effects. To distinguish the relative importance of the positive and negative cells, a positive cell alone is added in Case 3 (Figures 3e1 and 3f1). Both Cases 2 and 3 possess stronger PNJ cores than Case 1, consistent with the stronger jet in QBOe (Figure 2c).

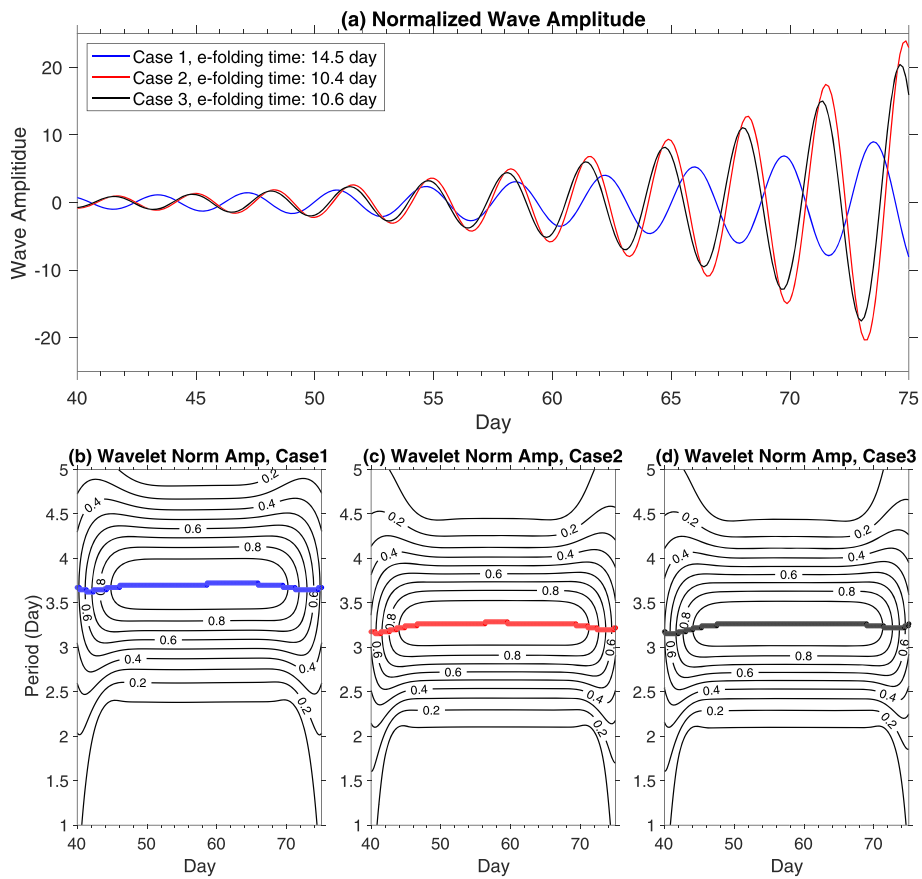


Figure 4. (a) Time evolutions of the EPW1 for Cases 1–3. Wave oscillations are normalized to wave amplitudes in the first wave cycles. (b–d) Wavelet spectra in wave amplitudes for Cases 1–3. Colored lines denote peak periods.

The same initial condition in the form of a random disturbance with wave number 1 is introduced at 65°S and 40 km for all three cases, which gradually evolves to the EPW motion (second to fifth rows of Figure 3). After 15 days, wave structure and growth rates remain nearly constant and model becomes stable. Considering that the results are from a simplified linear model, the overall wave structure agrees well with observations and especially, the wave phases after day 15 qualitatively approach the reality (Lu et al., 2013). The maximum wave amplitudes grow from ~10 to ~200 (unit is arbitrary) in Case 1, and from ~10 to ~500 in Cases 2 and 3.

We choose days 40–75 during which the model is fully stable to compute the *e*-folding time of wave amplitude increase. The wave oscillation is normalized to the maximum amplitude in the first wave cycle beginning in day 40 for all cases (Figure 4a). The wave evolutions in Cases 2 and 3 are comparable while different from Case 1. The growth rates for the three cases are $1/14.5$, $1/10.4$, and $1/10.6 \text{ day}^{-1}$, respectively, consistent with the slower growth rate in Case 1 shown in Figure 3. Aiming to diagnose the wave period that can explain the different wave phase behaviors, we divide the wave oscillation by its absolute amplitude to remove the effect of its exponential growth. The wavelet spectra show that wave period is ~3.7 day for Case 1, and ~3.3 day for Cases 2 and 3 (Figures 4b–4d). These waves represent polar unstable modes excited by the PNJ barotropic/baroclinic instabilities that have the fastest growth rates beating other wave components. Hartmann (1983) has also found that by simply increasing the PNJ strength without modifying its structure, the growth rate increases while wave period decreases, supporting our results. The differences between Cases 2 and 3 are negligible, while Case 1 shows smaller wave amplitude and longer period. The mechanism study suggests that during QBOe, the poleward flank PNJ is strengthened, leading to stronger \bar{u} that generates stronger EPW1 in the Antarctic 40- to 80-km region than that in QBOW. The effect from the negative cell is negligible.

4. Conclusions and Discussion

The 16 years of SABER temperature and geopotential height observations and MERRA-2 data are used to examine the interannual variability of 2–5d EPW1 and PNJ in the Antarctic austral winter. The positive correlation is found between the wave amplitude averaged over 50–82°S and PNJ strength averaged over $67.5 \pm 10^\circ\text{S}$, which are both featured by QBO-like signals. Both wave amplitudes and zonal-mean zonal winds follow the QBO more closely in the first 9 years than later, which implies that other processes may play a role afterward. The multiyear-averaged wave amplitudes in QBOe are about ~20% stronger than those in QBOw. Interannual variations of wave amplitudes from QBOw to QBOe can be more than twice as big. Compared to QBOw, the PNJ during QBOe weakens in the equatorward flank but strengthens in the poleward flank, forming a dipole-cell pattern in QBOe-QBOw differences. In the NH January, however, only one negative cell is found that has been explained by the Holton-Tan theory in previous studies. The mechanism for generating such a SH dipole-cell pattern, especially the positive cell in Antarctica, deserves further investigation.

We incorporate the QBO-related dipole-cell difference into the background wind to the linear mechanistic quasi-geostrophic model and simulate the EPW1 generation under different conditions of the PNJ. The stronger polar flank of the PNJ during QBOe over Antarctica is critical to generate the EPW1 with shorter periods and larger growth rates, which potentially leads to larger wave amplitude than during QBOw. The modeling results suggest a first-order mechanism that the equatorial QBO affects the mean wind in the polar region and then alters the efficiency of extracting energy from the mean wind to generate EPWs, thereby imposing the QBO signal onto the polar EPWs. Chu et al. (2018) have shown that potential energy densities of stratospheric gravity waves observed at McMurdo, Antarctica, are larger in 2012 and 2015 winters than 2011, 2013, and 2014, which is opposite to EPW1 interannual variability. Such QBO-like signature in gravity waves is likely caused by the filtering effect of the PNJ (X. Chu, private communication, 2019). Therefore, the coupling processes of the equatorial QBO signal to different types of polar waves can be multifold, and the nonlinear interaction and feedback between waves and mean flow should be considered in the future.

Acknowledgments

X. L.'s work was supported by NSF grants AGS-1705448, OPP-1705450, and CAREER-1753214. X. C. was partially supported by NSF grants OPP-1246405, OPP-1443726, and AGS-1452351. We acknowledge MERRA-2 data provided by the Global Modeling and Assimilation Office at NASA Goddard Space Flight Center. SABER data were downloaded from <http://saber.gats-inc.com/data.php>. This work's data are available at <https://zenodo.org/record/3493760#.XaeBxC2ZNbg>.

References

- Alexander, S. P., & Shepherd, M. G. (2010). Planetary wave activity in the polar lower stratosphere. *Atmospheric Chemistry and Physics*, 10(2), 707–718.
- Allen, D. R., Stanford, J. L., Elson, L. S., Fishbein, E. F., Froidevaux, L., & Waters, J. W. (1997). The 4-day wave as observed from the Upper Atmosphere Research Satellite Microwave Limb Sounder. *Journal of the Atmospheric Sciences*, 54, 420–434. [https://doi.org/10.1175/1520-0469\(1997\)054<0420:TDWAOF>2.0.CO;2](https://doi.org/10.1175/1520-0469(1997)054<0420:TDWAOF>2.0.CO;2)
- Baldwin, M. P., & Dunkerton, T. J. (1998a). Biennial, quasi-biennial, and decadal oscillations of potential vorticity in the northern stratosphere. *Journal of Geophysical Research*, 103, 3919–3928.
- Baldwin, M. P., & Dunkerton, T. J. (1998b). Quasi-biennial modulations of the Southern Hemisphere stratospheric polar vortex. *Geophysical Research Letters*, 25, 3343–3346.
- Baldwin, M. P., Gray, L. J., Dunkerton, T. J., Hamilton, K., Haynes, P. H., Randel, W. J., et al. (2001). The quasi-biennial oscillation. *Reviews of Geophysics*, 39, 170–229.
- Baumgaertner, A. J. G., McDonald, A. J., Hibbins, R. E., Fritts, D. C., Murphy, D. J., & Vincent, R. A. (2008). Short-period planetary waves in the Antarctic middle atmosphere. *Journal of Atmospheric and Solar-Terrestrial Physics*, 70, 1336. <https://doi.org/10.1016/j.jastp.2008.04.007>
- Becker, E. (2017). Mean-flow effects of thermal tides in the mesosphere and lower thermosphere. *Journal of the Atmospheric Sciences*, 74, 2043–2063. <https://doi.org/10.1175/JAS-D-16-0194.1>
- Chang, L. C., Palo, S. E., Liu, H.-L., Fang, T.-W., & Lin, C. S. (2010). Response of the thermosphere and ionosphere to an ultra fast Kelvin wave. *Journal of Geophysical Research*, 115, A00G04. <https://doi.org/10.1029/2010JA015453>
- Charney, J. G., & Drazin, P. G. (1961). Propagation of planetary-scale disturbances from the lower into the upper atmosphere. *Journal of Geophysical Research*, 66, 83–109.
- Chu, X., Zhao, J., Lu, X., Harvey, V. L., Jones, R. M., Becker, E., et al. (2018). Lidar observations of stratospheric gravity waves from 2011 to 2015 at McMurdo ($77.84^\circ\text{S}, 166.69^\circ\text{E}$), Antarctica: 2. Potential energy densities, lognormal distributions, and seasonal variations. *Journal of Geophysical Research: Atmospheres*, 123(15), 7910–7934. <https://doi.org/10.1029/2017JD027386>
- Coy, L., Stajner, I., Dasilva, A. M., Joiner, J., Rood, R. B., Pawson, S., & Lin, S. J. (2003). High-frequency planetary waves in the polar middle atmosphere as seen in a data assimilation system. *Journal of the Atmospheric Sciences*, 60, 2975. [https://doi.org/10.1175/1520-0469\(2003\)060<2975:HPWITP>2.0.CO;2](https://doi.org/10.1175/1520-0469(2003)060<2975:HPWITP>2.0.CO;2)
- Coy, L., Wargan, K., Molod, A. M., McCarty, W. R., & Pawson, S. (2016). Structure and dynamics of the quasi-biennial oscillation in MERRA-2. *Journal of Climate*, 29(No14), 5339–5354. <https://doi.org/10.1175/JCLI-D-15-0809.1>
- Dunkerton, T. J., & Baldwin, M. P. (1991). Quasi-biennial modulation of planetary wave fluxes in the Northern Hemisphere winter. *Journal of the Atmospheric Sciences*, 48, 1043–1061.
- Dunkerton, T. J., & Delisi, D. P. (1985). Climatology of the equatorial lower stratosphere. *Journal of the Atmospheric Sciences*, 42, 376–396.
- Forbes, J. M., Zhang, X. L., Palo, S. E., Russell, J., Mertens, C. J., & Mlynczak, M. (2009). Kelvin waves in stratosphere, mesosphere and lower thermosphere temperatures as observed by TIMED/SABER during 2002–2006. *Earth, Planets and Space*, 61(4), 447–453.
- Garcia, R. R., Lieberman, R., Russell, J. M., & Mlynczak, M. G. (2005). Large-scale waves in the mesosphere and lower thermosphere observed by SABER. *Journal of the Atmospheric Sciences*, 62, 4384–4439.

- Gelaro, R., McCarty, W., Suárez, M. J., Todling, R., Molod, A., Takacs, L., et al. (2017). The Modern-Era Retrospective Analysis for Research and Applications, version 2 (MERRA-2). *Journal of Climate*, 30(14), 5419–5454. <https://doi.org/10.1175/JCLI-D-16-0758.1>
- Gu, S.-Y., Dou, X., Lei, J., Li, T., Luan, X., Wan, W., & Russell, J. M. (2014). Ionospheric response to the ultrafast Kelvin wave in the MLT region. *Journal of Geophysical Research: Space Physics*, 119, 1369–1380. <https://doi.org/10.1002/2013JA019086>
- Hamilton, K. (1998). Effects of an imposed quasi-biennial oscillation in a comprehensive troposphere-stratosphere-mesosphere general circulation model. *Journal of the Atmospheric Sciences*, 55, 2393–2418.
- Hartmann, D. L. (1979). Baroclinic instability of realistic zonal-mean states to planetary waves. *Journal of the Atmospheric Sciences*, 36, 2336–2349.
- Hartmann, D. L. (1983). Barotropic instability of the polar night jet stream. *Journal of the Atmospheric Sciences*, 40, 817. [https://doi.org/10.1175/1520-0469\(1983\)040<0817:BIOTPN>2.0.CO;2](https://doi.org/10.1175/1520-0469(1983)040<0817:BIOTPN>2.0.CO;2)
- Holton, J. R., & Tan, H. C. (1980). The influence of the equatorial quasi-biennial oscillation on the global circulation at 50 mb. *Journal of the Atmospheric Sciences*, 37, 2200–2208.
- Labitzke, K. (1982). On the interannual variability of the middle stratosphere during the northern winters. *Journal of the Meteorological Society of Japan*, 60, 124–139.
- Lawrence, B. N., Fraser, G. J., Vincent, R. A., & Philips, A. (1995). The 4-day wave in the Antarctic mesosphere. *Journal of Geophysical Research*, 100, 18899. <https://doi.org/10.1029/95JD01168>
- Lu, X., Chu, X., Chen, C., Nguyen, V., & Smith, A. K. (2017). First observations of short-period eastward propagating planetary waves from the stratosphere to the lower thermosphere (110 km) in winter Antarctica. *Geophysical Research Letters*, 44, 10,744–10,753. <https://doi.org/10.1002/2017GL075641>
- Lu, X., Chu, X., Fuller-Rowell, T., Chang, L., Fong, W., & Yu, Z. (2013). Eastward propagating planetary waves with periods of 1–5 days in the winter Antarctic stratosphere as revealed by MERRA and lidar. *Journal of Geophysical Research: Atmospheres*, 118, 9565–9578. <https://doi.org/10.1002/jgrd.50717>
- Lu, X., Wu, H., Oberheide, J., Liu, H., & McInerney, J. (2018). Latitudinal double-peak structure of stationary planetary wave 1 in the austral winter middle atmosphere and its possible generation mechanism. *Journal of Geophysical Research: Atmospheres*, 123, 11,551–11,568. <https://doi.org/10.1029/2018JD029172>
- Manney, G. L., Orsolini, Y. J., Pumphrey, H. C., & Roche, A. E. (1998). The 4-day wave and transport of UARS tracers in the austral polar vortex. *Journal of the Atmospheric Sciences*, 55, 3456. [https://doi.org/10.1175/1520-0469\(1998\)055<3456:TDWATO>2.0.CO;2](https://doi.org/10.1175/1520-0469(1998)055<3456:TDWATO>2.0.CO;2)
- Manney, G. L., & Randel, W. J. (1993). Instability at the winter stratopause: A mechanism for the 4-day wave. *Journal of the Atmospheric Sciences*, 50, 3,928. [https://doi.org/10.1175/15200469\(1993\)050<3928:IATWSA>2.0.CO;2](https://doi.org/10.1175/15200469(1993)050<3928:IATWSA>2.0.CO;2)
- McLandress, C., Ward, W. E., Fomichev, V. I., Semeniuk, K., Beagley, S. R., McFarlane, N. A., & Shepherd, T. G. (2006). Large-scale dynamics of the mesosphere and lower thermosphere: An analysis using the extended Canadian Middle Atmosphere Model. *Journal of Geophysical Research*, 111, D17111. <https://doi.org/10.1029/2005JD006776>
- O'Sullivan, D., & Salby, M. L. (1990). Coupling of the quasi-biennial oscillation and the extratropical circulation in the stratosphere through planetary wave transport. *Journal of the Atmospheric Sciences*, 47, 650–673.
- Rossby, C. G., & Collaborators (1939). Relation between variations in the intensity of the zonal circulation of the atmosphere and the displacements of the semi-permanent centers of action. *Journal of Marine Research*, 2(1), 38–55. <https://doi.org/10.1357/00222403980649023>
- Russell, J. M., Mlynczak, M. G., Gordley, L. L., Tansock, J. J., & Esplin, R. W. (1999). Overview of the SABER experiment and preliminary calibration results. *Proceedings of SPIE The International Society for Optical Engineering*, 3756, 277–288. <https://doi.org/10.1117/12.366382>
- Smith, A. K. (2003). The origin of stationary planetary waves in the upper mesosphere. *Journal of the Atmospheric Sciences*, 60, 3033–3041.
- Venne, D. E., & Stanford, J. L. (1982). An observational study of high-latitude stratospheric planetary waves in winter. *Journal of the Atmospheric Sciences*, 39, 1026–1034. [https://doi.org/10.1175/1520-0469\(1982\)039<1026:AOSOHL>2.0.CO;2](https://doi.org/10.1175/1520-0469(1982)039<1026:AOSOHL>2.0.CO;2)
- Watanabe, S., Tomikawa, Y., Sato, K., Kawatani, Y., Miyazaki, K., & Takahashi, M. (2009). Simulation of the eastward 4-day wave in the Antarctic winter mesosphere using a gravity wave resolving general circulation model. *Journal of Geophysical Research*, 114, D16111. <https://doi.org/10.1029/2008JD011636>
- Zhang, X., Forbes, J. M., & Hagan, M. E. (2010). Longitudinal variation of tides in the MLT region: 1. Tides driven by tropospheric net radiative heating. *Journal of Geophysical Research*, 115, A06316. <https://doi.org/10.1029/2009JA014897>